

The Fermi Bubbles as a Scaled-up Version of Supernova Remnants

Yutaka Fujita

*Department of Earth and Space Science, Graduate School of Science, Osaka University,
Toyonaka, Osaka 560-0043, Japan*

fujita@vega.ess.sci.osaka-u.ac.jp

and

Yutaka Ohira and Ryo Yamazaki

*Department of Physics and Mathematics, Aoyama Gakuin University, Fuchinobe,
Chuou-ku, Sagamihara 252-5258, Japan*

ABSTRACT

In this study, we treat the Fermi bubbles as a scaled-up version of supernova remnants (SNRs). The bubbles are created through activities of the supermassive black hole (SMBH) or starbursts at the Galactic center (GC). Cosmic rays (CRs) are accelerated at the forward shocks of the bubbles like SNRs, which means that we cannot decide whether the bubbles were created by the SMBH or starbursts from the radiation from the CRs. We follow the evolution of CR distribution by solving a diffusion-advection equation, considering the reduction of the diffusion coefficient by CR streaming. In this model, gamma-rays are created through hadronic interaction between CR protons and the gas in the Galactic halo. In the GeV band, we can well reproduce the observed flat distribution of gamma-ray surface brightness, because some amount of gas is left behind the shock. The edge of the bubbles is fairly sharp owing to the high gas density behind the shock and the reduction of the diffusion coefficient there. The latter also contributes the hard gamma-ray spectrum of the bubbles. We find that the CR acceleration at the shock has started when the bubbles were small, and the time-scale of the energy injection at the GC was much smaller than the age of the bubbles. We predict that if CRs are accelerated to the TeV regime, the apparent bubble size should be larger in the TeV band, which could be used to discriminate our hadronic model from other leptonic models. We also present neutrino fluxes.

Subject headings: cosmic rays — galaxies: active — galaxies: starburst — gamma rays: galaxies — ISM: supernova remnants

1. Introduction

The Fermi bubbles are huge gamma-ray bubbles discovered with *Fermi Gamma-ray Space Telescope* in the direction of the Galactic center (GC) in the GeV band (Su, Slatyer, & Finkbeiner 2010; see also Dobler et al. 2010). They are symmetric about the Galactic plane and the size is $\sim 50^\circ$ (~ 10 kpc). Their surface brightness is relatively uniform, and they have sharp edges and hard spectrum (Su et al. 2010).

Several models have been proposed for the origin of the bubbles. These models assume that activities of the super-massive black hole (SMBH) or starbursts at the GC created the bubbles. Some models indicated that cosmic-rays (CR) that are accelerated via star formation activities are conveyed into the bubbles (Crocker & Aharonian 2011; Crocker 2012). Others pointed out that the CRs are originated from jets launched by the central black hole (Guo & Mathews 2012), or accelerated inside the bubbles (Mertsch & Sarkar 2011; Cheng et al. 2011). Gamma-rays can be generated by interaction between CR protons and ambient gas (hadronic models), or by inverse Compton scattering by CR electrons (leptonic models).

In this study, we treat the Fermi bubbles as a scaled-up version of supernova remnants (SNRs). CRs are accelerated at the forward shock front like SNRs. We explicitly solve a diffusion-advection equation to study the evolution of CR distribution. We also focus on the reduction of the diffusion coefficient around the bubbles, which slows CR diffusion and is crucial to explain the sharp edge of the bubbles (Guo et al. 2012). The reduction has been indicated and studied for SNRs (Torres et al. 2008; Fujita et al. 2009; Li & Chen 2010; Ohira, Murase, & Yamazaki 2011; Fujita et al. 2011; Yan, Lazarian, & Schlickeiser 2012; Nava & Gabici 2013; Malkov et al. 2013); it could be caused by a CR streaming instability or anisotropic diffusion. For the Fermi bubbles, Yang et al. (2012) studied the reduction by the latter. In this study, we investigate the former. We refer to protons as CRs unless otherwise mentioned.

2. Models

For the sake of simplicity, we assume a spherically symmetric bubble, and mainly focus on the high-galactic-latitude part of the Fermi bubbles (large $|b|$ and small $|l|$ in the Galactic coordinate). Before the bubble is born, the gas in the Galactic halo is static and has a distribution of $\rho_0(r) = \rho_1(r/r_1)^{-\omega}$, where r is the distance from the GC, and ρ_1 , r_1 , and ω are the parameters. We assume that the adiabatic index of the gas is $\gamma = 5/3$. For hydrodynamic evolution of the halo gas, we adopt the Sedov-Taylor solution (e.g. Mihalas & Mihalas 1984; Ostriker & McKee 1988). If an energy is injected at $t = 0$ at the GC, the radius of the shock

front of the bubble can be written as

$$R_{\text{sh}}(t) = \xi \left(\frac{E_{\text{tot}}}{\rho_1 r_1^\omega} \right)^{1/(5-\omega)} t^{2/(5-\omega)}, \quad (1)$$

where $\xi \sim 1$, and E_{tot} is the injected energy. On the other hand, if the energy is continuously injected at a rate of L_w at the GC, it should be

$$R_{\text{sh}}(t) = \xi \left(\frac{L_w}{\rho_1 r_1^\omega} \right)^{1/(5-\omega)} t^{3/(5-\omega)}. \quad (2)$$

We ignore the effect of CR pressure on the gas. We do not care about the energy source: it may be the SMBH or starburst activities at the GC. If the gas has a finite temperature, the Mach number of the shock gradually decreases as the velocity, $V_{\text{sh}} = dR_{\text{sh}}/dt$, decreases. The gas density ρ and velocity u for $r < R_{\text{sh}}$ follow the Sedov-Taylor solution.

Our CR model is based on the one in Fujita, Ohira, & Takahara (2010) for the evolution of SNRs. However, while we adopted a Monte Carlo approach in Fujita et al. (2010) to calculate the CR distribution, in this study we explicitly solve a diffusion-advection equation to follow the evolution of a CR distribution function $f(r, p, t)$, where p is the momentum of CRs. The equation is

$$\frac{\partial f}{\partial t} = \frac{1}{r^2} \frac{\partial}{\partial r} \left(r^2 \kappa \frac{\partial f}{\partial r} \right) - (u + u_w) \frac{\partial f}{\partial r} + \frac{1}{3r^2} \left[\frac{\partial}{\partial r} (r^2 (u + u_w)) \right] p \frac{\partial f}{\partial p} + Q, \quad (3)$$

where the source Q describes particle injection, and u_w is the velocity of the waves that scatter CRs. We assume that $u_w = v_A$ for $r > R_{\text{sh}}$, where v_A is the Alfvén velocity, and that $u_w = 0$ for $r < R_{\text{sh}}$ because the waves would isotropically propagate for $r < R_{\text{sh}}$.

CRs are accelerated at the shock front of the bubble ($r = R_{\text{sh}}$). We do not consider the details of particle acceleration. CRs are accelerated in the shock neighborhood, where some nonlinear effects generate strong magnetic waves or cause strong amplification of magnetic fields (Lucek & Bell 2000; Bell 2004). In this region, particle diffusion would follow the so-called Bohm diffusion and CR acceleration is effective. The spatial scale of the region is much smaller than R_{sh} and we ignore the width. Thus, we assume that

$$Q(r, p, t) = \begin{cases} K_Q^{-1} p^{-q} \rho(R_{\text{sh},+}) V_{\text{sh}}^3 \delta(r - R_{\text{sh}}) & \text{if } p_{\text{min}} < p < p_{\text{max}} \\ 0 & \text{otherwise,} \end{cases} \quad (4)$$

where q is the parameter, and $R_{\text{sh},+}$ is the radius just outside the shock. At a strong shock, the standard diffusive shock acceleration model predicts that $q \sim 4$ (Drury 1983). For instant energy injection (equation (1)), the coefficient is written as

$$K_Q = 16\pi^2 c \xi^{5-\omega} \left(\frac{2}{5-\omega} \right)^3 \frac{E_{\text{tot}}}{E_{\text{cr,tot}}} \ln \left(\frac{t_f}{t_0} \right) \int_{p_{\text{min}}}^{p_{\text{max}}} p'^{2-q} \sqrt{p'^2 + m_p^2 c^2} dp', \quad (5)$$

while for constant energy injection (equation (2)), it is written as

$$K_Q = 16\pi^2 c \xi^{5-\omega} \left(\frac{3}{5-\omega} \right)^3 \frac{L_w}{E_{\text{cr,tot}}} (t_f - t_0) \int_{p_{\text{min}}}^{p_{\text{max}}} p'^{2-q} \sqrt{p'^2 + m_p^2 c^2} dp', \quad (6)$$

where c is the light velocity, and m_p is the proton mass. CRs are accelerated and injected into the Galactic halo space between $t = t_0$ and t_f , and $E_{\text{cr,tot}}$ is the total energy of the CRs accelerated during that period. The maximum momentum $p_{\text{max}}(t)$ is determined by the condition of $t_{\text{acc}} = t_{\text{age}}$, where t_{acc} is the acceleration time-scale and t_{age} is the age of the bubble. In our case, $t_{\text{age}} = t$ and

$$p_{\text{max}} \approx \frac{3}{20} \frac{eB_0}{\eta_g c^2} V_{\text{sh}}^2 t, \quad (7)$$

where e is the proton charge, B_0 is the background magnetic field, and η_g is the gyro-factor (Aharonian & Atoyan 1999; Ohira et al. 2010). We assume that the shock is strong. Unless otherwise mentioned, we assume $\eta_g = 1$ (Bohm diffusion). Instead of equation (7), p_{max} is often determined by an escape condition for SNRs (Ptuskin & Zirakashvili 2005; Reville et al. 2009). This is because the characteristic spatial length of particles penetrating into the shock upstream region can be comparable to the size of SNRs (Ohira et al. 2010). However, this cannot be applied to the Fermi bubbles, because the size of the bubbles is much larger than the characteristic length. We fix the minimum momentum at $p_{\text{min}} = m_p c$.

The CRs escaped from the shock neighborhood may amplify magnetic fluctuations (Alfvén waves) in the Galactic halo through a streaming instability (Wentzel 1974; Skilling 1975). Since CRs are scattered by the fluctuations, the diffusion coefficient κ in equation (3) is reduced. At the rest frame and outside the bubble ($r \geq R_{\text{sh}}$), the wave growth is given by

$$\frac{\partial \psi}{\partial t} = \frac{4\pi v_{\text{A}} p^4 v}{3 U_M} |\nabla f|, \quad (8)$$

where $\psi(r, p, t)$ is the energy density of Alfvén waves per unit logarithmic bandwidth (which are resonant with particles of momentum p) relative to the ambient magnetic energy density U_M (Bell 1978), and v is the particle velocity. The diffusion coefficient is simply given as

$$\kappa(r, p, t) = \frac{4}{3\pi} \frac{pvc}{eB_0\psi}. \quad (9)$$

Within the bubble, the evolution of the waves could be complicated, because it could be controlled by something like turbulence. Thus for $r < R_{\text{sh}}$, we simply assume that

$$\kappa(r, p, t) = \kappa_B \rho(R_{\text{sh}}) / \rho(r), \quad (10)$$

where $\kappa_B = \eta_g pc^2 / (3eB)$ is a Bohm-type diffusion coefficient (Berezhko et al. 1994), and $B \approx 4B_0$ for a strong shock. The results do not much depend on the diffusion coefficient inside the bubble if it is small enough. Although there is no strong observational constraint on magnetic fields in the Galactic halo, we assume that they are given by $B_0(r) = B_1(r/r_1)^{-\omega/2}$. For the value of $B_1 = 10 \mu\text{G}$, the Alfvén velocity has a constant value of $v_A = B_0 / \sqrt{4\pi\rho} = 100 \text{kms}^{-1}$. The field strength we assumed is comparable to or smaller than the value adopted by Su et al. (2010) or $B = 30 e^{-r/2 \text{kpc}} \mu\text{G}$ for $r \lesssim 10 \text{kpc}$. Gamma-ray and neutrino fluxes created through hadronic interactions between CR protons and gas protons are calculated using the code provided by Karlsson & Kamae (2008).

We consider four models. Model FD is our fiducial model; an energy of $E_{\text{tot}} = 2.5 \times 10^{57} \text{ erg}$ is instantaneously released at $t = 0$ at $r = 0$ (see equation (1)). For the initial distribution of the halo gas, we assume that $\omega = 1.5$, $\rho_1 = 7.8 \times 10^{-24} \text{ g cm}^{-3}$ and $r_1 = 0.1 \text{ kpc}$ to be consistent with gamma-ray observations (Section 3). The index $\omega = 1.5$ is an approximation of the profile obtained by Guo & Mathews (2012). We solve equations (3) and (8) for $t \geq t_0 = 1 \times 10^6 \text{ yr}$. It is to be noted that if the SMBH at the GC injects energy at a rate of 16% of the Eddington luminosity ($\sim 5 \times 10^{44} \text{ erg s}^{-1}$) for $1 \times 10^6 \text{ yr}$, the total energy is comparable to E_{tot} . The energy that goes into CRs is $E_{\text{cr,tot}} = 0.2 E_{\text{tot}}$ in total. The spectral index of the accelerated CRs is assumed to be $q = 4.1$. For the parameters we adopted, the maximum momentum at $t = t_0$ is $p_{\text{max}}c = 9 \times 10^{14} \text{ eV}$. At $t = t_0$, we assume that the diffusion coefficient has typical Galactic values:

$$\kappa_i = 10^{28} \left(\frac{E}{10 \text{ GeV}} \right)^{0.5} \left(\frac{B_0}{3 \mu\text{G}} \right)^{-0.5} \text{ cm}^2 \text{ s}^{-1}, \quad (11)$$

where E is the energy of a CR proton (Gabici et al. 2009). From equation (9), we obtain the initial wave energy density $\psi_i(r, p) = \psi(r, p, t_0) \propto \kappa_i^{-1}$. If the temperature of the halo gas is $T = 2.4 \times 10^6 \text{ K}$ (Guo & Mathews 2012), the Mach number of the shock at $t = 3 \times 10^6 \text{ yr}$ is $\mathcal{M} \sim 4$. Since it is generally believed that CR acceleration is ineffective at smaller Mach numbers (e.g. Gieseler et al. 2000), we assume that CR acceleration finishes at $t_f = 3 \times 10^6 \text{ yr}$. The current age of the bubble is assumed to be $t_{\text{obs}} = 10^7 \text{ yr}$ and the bubble center (GC) is located at a distance of 8.5 kpc. The current bubble size is $R_{\text{sh}}(t_{\text{obs}}) = 9.7 \text{ kpc}$.

Other models are studied for comparison. Their parameters are the same as those for Model FD except for the followings. In Model NG, the wave growth is ignored, and we assume that $\kappa = \kappa_i$ for $r > R_{\text{sh}}$. In Model LA, acceleration of CRs starts later, and we adopt $t_0 = 4 \times 10^6 \text{ yr}$ and $t_f = t_{\text{obs}} = 10^7 \text{ yr}$. In Model CI, energy is continuously injected from the GC at a rate of $L_w = E_{\text{tot}}/t_{\text{obs}}$ for $t < t_{\text{obs}}$ (see equation (2)), and we set $t_{\text{obs}} = 2 \times 10^7 \text{ yr}$ so that the position of the peak of the surface brightness profiles is almost the same as that of Model FD.

3. Results

Figure 1 shows the surface brightness profiles of the bubble. They are calculated simply by projecting gamma-ray emissions on a plane at a distance of 8.5 kpc and we do not consider the detailed geometrical effects that come up when the distance to the Fermi bubbles is finite. Figure 1a shows the results for Model FD, which are compared with the southern bubble data in Figure 9 in Su et al. (2010); one degree corresponds to $\pi/180 \times 8.5$ kpc. Since our model is rather simple and we do not include background, we shift the observational data along the horizontal axis ($+5^\circ$) and the vertical axis ($-0.9 \text{ keV cm}^{-2} \text{ s}^{-1} \text{ sr}^{-1}$ in the 1–5 GeV band and $-0.4 \text{ keV cm}^{-2} \text{ s}^{-1} \text{ sr}^{-1}$ in the 5–20 band). At 2 and 10 GeV, the predicted profiles are fairly flat and have sharp edges at $r \sim 50^\circ$ as observations suggest (Figure 1a). Significant gamma-ray emissions fill the bubble, because not all the gas is concentrated at the shock. (Model FD in Figure 2).

The sharp edges seen in Figure 1a are created by the dense gas just behind the shock. Moreover, the wave amplification outside the shock also contributes to the formation of the sharp edges. Figure 3 shows the wave amplification ψ/ψ_i at $r = R_{\text{sh},+}$ and $t = t_{\text{obs}}$ for Model FD. The amplification leads to the decrease of the diffusion coefficient (equation (9)) and slows the CR diffusion out of the bubble. While the wave energy ψ grows at a given radius outside the shock (equation (8)), the wave energy at the expanding shock ($r = R_{\text{sh},+}(t)$) gradually decreases. While ψ/ψ_i is not much dependent on CR momentum at $10^{10} \lesssim pc \lesssim 10^{14}$ eV (Figure 3), $\psi_i \propto \kappa_i^{-1}$ is a decreasing function of CR momentum (equations (9) and (11)). This means that $\kappa \propto \psi^{-1}$ is an increasing function of CR momentum and CRs with larger energies diffuse faster. Assuming that CR acceleration stopped at $t = t_f < t_{\text{obs}}$, CRs are left far behind the shock at $t = t_{\text{obs}}$ if their diffusion is not much effective. This happens for GeV CRs in Model FD; most of them remain far behind the shock. However, this is not the case for CRs with much larger energies. At $t = t_{\text{obs}}$ and $r = R_{\text{sh},+}$, the diffusion coefficient for CRs with $pc = 10$ TeV is $\kappa = 9.7 \times 10^{28} \text{ cm}^2 \text{ s}^{-1}$. Thus, the diffusion scale-length is $l_{\text{diff}} \sim \sqrt{4\kappa(t_{\text{obs}} - t_f)} \sim 3.0$ kpc. On the other hand, the shock velocity at $t = t_{\text{obs}}$ is $V_{\text{sh}} = 540 \text{ km s}^{-1}$, and thus the advection scale-length is $l_{\text{adv}} = V_{\text{sh}}(t_{\text{obs}} - t_f) \sim 3.9$ kpc. Since $l_{\text{diff}} \lesssim l_{\text{adv}}$, most CRs do not diffuse beyond the shock radius, although the diffusion cannot be ignored. This explains the profile of 1 TeV gamma-rays, which is created by CRs with ~ 10 TeV (Figure 1a). The moderate diffusion enables some of the TeV CRs to reach the very high density region just behind the shock. This makes the surface brightness at 1 TeV a little brighter than those at smaller energies (Figure 1a). We note that the slight increase of ψ/ψ_i at $pc \sim 10^{14}$ eV in Figure 3 is caused by the higher-energy CRs that have arrived at $r \sim R_{\text{sh}}$. In Model NG, in which the wave growth is ignored, the diffusion for GeV CRs is the moderate one and the surface brightness in the GeV band is larger than that for Model FD (Figure 1b). However, the diffusion of CRs with \gtrsim TeV is much faster and the

CRs diffuse beyond the shock radius (Figure 1b). While the surface brightness profile for a given energy is relatively flat for Model NG, the spatial extension of CRs varies with their energies because of the fairly large and energy-dependent diffusion (equation (11)).

In Model LA, the limb-brightening becomes more prominent because CRs do not have much time to diffuse out (Figure 1b). Thus, t_0 must be much smaller than t_{obs} , or CR acceleration must have started at the shock when the bubble is small. The observed flatness of the surface brightness profiles may also imply that the time-scale of the energy injection at the GC is much shorter than the age of the bubble ($t_{\text{inj}} \ll t_{\text{obs}}$). In Models FD, NG and LA, we implicitly assumed that $t_{\text{inj}} \lesssim t_0$. On the other hand, in Model CI the energy has been continuously injected at the GC ($t_{\text{inj}} = t_{\text{obs}}$). In this case, the halo gas inside the bubble ($r < R_{\text{sh}}$) is compressed into a thin dense shell between the shock and the contact discontinuity at $r = 0.86 R_{\text{sh}}$ (Figure 2). If the region behind the contact discontinuity ($r < 0.86 R_{\text{sh}}$) is almost empty with gas, the gamma-ray image should have a shell-like structure (Model CI in Figure 1b), because gamma-rays are created through the interaction between CRs and the gas of the thin shell. In Model CI, we assume that the gas density inside the contact discontinuity is $0.1 \rho(R_{\text{sh},+})$ for a calculational purpose.

Figure 4 shows the gamma-ray spectrum of the bubble for Model FD. The observed hard gamma-ray spectrum is reproduced, which reflects that the spectral index of the CRs around the bubble is not much different from the original one ($q = 4.1$). This is because of the decrease of the diffusion coefficient or the confinement of CRs around the bubble. For Model NG, the confinement depends on CR energies, and the original CR spectrum is not conserved (Ohira et al. 2011). In Figure 4, the gamma-ray luminosity in the TeV band is slightly larger than that in the GeV band as was shown in Figure 1a. We note that the TeV luminosity depends on p_{max} . For example, larger η_g makes p_{max} smaller (equation (7)). The dotted line in Figure 4 shows the spectrum when $\eta_g = 100$; other parameters are the same as those for Model FD. As can be seen, the TeV luminosity is much reduced. In Figure 4, we also present the neutrino spectrum for Model FD. The flux is similar to the one predicted by Lunardini & Razzaque (2012), and thus their discussion can be applied. Our results indicate that the neutrino flux is comparable to the background and it could be marginally detected (Lunardini & Razzaque 2012).

Model FD indicates that the position of the shock is a few kpc outside the edge of the gamma-ray bubble. X-ray emission from the high-density gas just behind the shock could have been detected there (Sofue 2000; Bland-Hawthorn & Cohen 2003). In Model FD, in which CRs are accelerated to PeV, we also predict that the size of the bubble is larger in the TeV band (Figure 1a), because of the faster diffusion of higher energy CRs. The difference of the size of the bubble between the GeV and TeV bands could be used to discriminate our

hadronic model from other leptonic models. In the leptonic models, gamma-rays originate from electrons and the cooling time of the electrons with energies of $\gtrsim 30$ GeV is smaller than the age of the bubbles (Figure 28 in Su et al. 2010). This means that the electrons must be being accelerated. Thus, the gamma-rays should be observed around the acceleration sites and the gamma-ray distribution should not depend on the energy band. In particular, since the cooling time of TeV electrons is very short ($\lesssim 10^6$ yr), the diffusion of the electrons can be ignored and the distribution of the gamma-rays from them should reflect the positions of the acceleration sites.

4. Summary and Discussion

We solve a diffusion-advection equation to investigate the evolution of the distribution of CRs accelerated at the shock front of the Fermi bubbles. We found that the observed flat surface brightness profile with a sharp edge can be reproduced because of the gas inside the bubbles and the reduced diffusion coefficient owing to CR streaming instabilities. The latter also contributes to the hard spectrum of the bubbles. The CR acceleration must have started at the early stage of the bubble evolution and the time-scale of energy injection at the GC must be much smaller than the current age of the bubbles.

the hadronic model by Crocker & Aharonian (2011), the bubbles are long-lived ($\gtrsim 8$ Gyr) or steady. This is not likely in our model because the forward shocks rapidly cross the halo ($\sim 10^7$ yr), unless the background gas is rapidly falling toward the galactic plane. If the SMBH blows winds, reverse shocks may develop in the winds (Zubovas, King, & Nayakshin 2011), and CRs may be accelerated there. Our model does not treat this type of acceleration. If the reverse shocks disappear in a short time, the situation may not be much different from the one we considered. Moreover, since the reverse shocks are located in the innermost region of the bubbles, it may take a longer time for the CRs accelerated there to diffuse out to the dense region at the bubble edge than those accelerated at the forward shocks. Thus, the contribution of the former to the gamma-ray emission may be less than that of the latter. Zubovas & Nayakshin (2012) indicated that the activity of the SMBH lasted $\sim 10^6$ yr and the current age of the bubbles is $\sim 10^7$ yr, which are consistent with our model. They also indicated that buoyancy may deform the bubbles. Although it may somewhat change the height of the bubbles, our results may not be much affected as long as CRs generally move with the background gas.

This work was supported by KAKENHI (YF: 23540308, YO: No.24.8344). R. Y. was supported by the fund from Research Institute, Aoyama Gakuin University.

REFERENCES

- Aharonian, F. A., & Atoyan, A. M. 1999, *A&A*, 351, 330
- Bell, A. R. 1978, *MNRAS*, 182, 147
- Bell, A. R. 2004, *MNRAS*, 353, 550
- Berezhko, E. G., Yelshin, V. K., & Ksenofontov, L. T. 1994, *Astroparticle Physics*, 2, 215
- Bland-Hawthorn, J., & Cohen, M. 2003, *ApJ*, 582, 246
- Cheng, K.-S., Chernyshov, D. O., Dogiel, V. A., Ko, C.-M., & Ip, W.-H. 2011, *ApJ*, 731, L17
- Crocker, R. M., & Aharonian, F. 2011, *Physical Review Letters*, 106, 101102
- Crocker, R. M. 2012, *MNRAS*, 423, 3512
- Dobler, G., Finkbeiner, D. P., Cholis, I., Slatyer, T., & Weiner, N. 2010, *ApJ*, 717, 825
- Drury, L. O. 1983, *Reports on Progress in Physics*, 46, 973
- Fujita, Y., Ohira, Y., & Takahara, F. 2010, *ApJ*, 712, L153
- Fujita, Y., Ohira, Y., Tanaka, S. J., & Takahara, F. 2009, *ApJ*, 707, L179
- Fujita, Y., Takahara, F., Ohira, Y., & Iwasaki, K. 2011, *MNRAS*, 415, 3434
- Gabici, S., Aharonian, F. A., & Casanova, S. 2009, *MNRAS*, 396, 1629
- Gieseler, U. D. J., Jones, T. W., & Kang, H. 2000, *A&A*, 364, 911
- Guo, F., & Mathews, W. G. 2012, *ApJ*, 756, 181
- Guo, F., Mathews, W. G., Dobler, G., & Oh, S. P. 2012, *ApJ*, 756, 182
- Karlsson, N., & Kamae, T. 2008, *ApJ*, 674, 278
- Li, H., & Chen, Y. 2010, *MNRAS*, 409, L35
- Lucek, S. G., & Bell, A. R. 2000, *MNRAS*, 314, 65
- Lunardini, C., & Razzaque, S. 2012, *Physical Review Letters*, 108, 221102
- Malkov, M. A., Diamond, P. H., Sagdeev, R. Z., Aharonian, F. A., & Moskalenko, I. V. 2013, *ApJ*, 768, 73

- Mertsch, P., & Sarkar, S. 2011, *Physical Review Letters*, 107, 091101
- Mihalas, D., & Mihalas, B. W. 1984, *Foundations of Radiation Hydrodynamics* (New York: Oxford University Press), § 60
- Nava, L., & Gabici, S. 2013, *MNRAS*, 429, 1643
- Ohira, Y., Murase, K., & Yamazaki, R. 2010, *A&A*, 513, A17
- Ohira, Y., Murase, K., & Yamazaki, R. 2011, *MNRAS*, 410, 1577
- Ostriker, J. P., & McKee, C. F. 1988, *Reviews of Modern Physics*, 60, 1
- Ptuskin, V. S., & Zirakashvili, V. N. 2005, *A&A*, 429, 755
- Reville, B., Kirk, J. G., & Duffy, P. 2009, *ApJ*, 694, 951
- Skilling, J. 1975, *MNRAS*, 173, 255
- Sofue, Y. 2000, *ApJ*, 540, 224
- Su, M., & Finkbeiner, D. P. 2012, *ApJ*, 753, 61
- Su, M., Slatyer, T. R., & Finkbeiner, D. P. 2010, *ApJ*, 724, 1044
- Torres, D. F., Rodriguez Marrero, A. Y., & de Cea Del Pozo, E. 2008, *MNRAS*, 387, L59
- Wentzel, D. G. 1974, *ARA&A*, 12, 71
- Yan, H., Lazarian, A., & Schlickeiser, R. 2012, *ApJ*, 745, 140
- Yang, H.-Y. K., Ruszkowski, M., Ricker, P. M., Zweibel, E., & Lee, D. 2012, *ApJ*, 761, 185
- Zubovas, K., King, A. R., & Nayakshin, S. 2011, *MNRAS*, 415, L21
- Zubovas, K., & Nayakshin, S. 2012, *MNRAS*, 424, 666

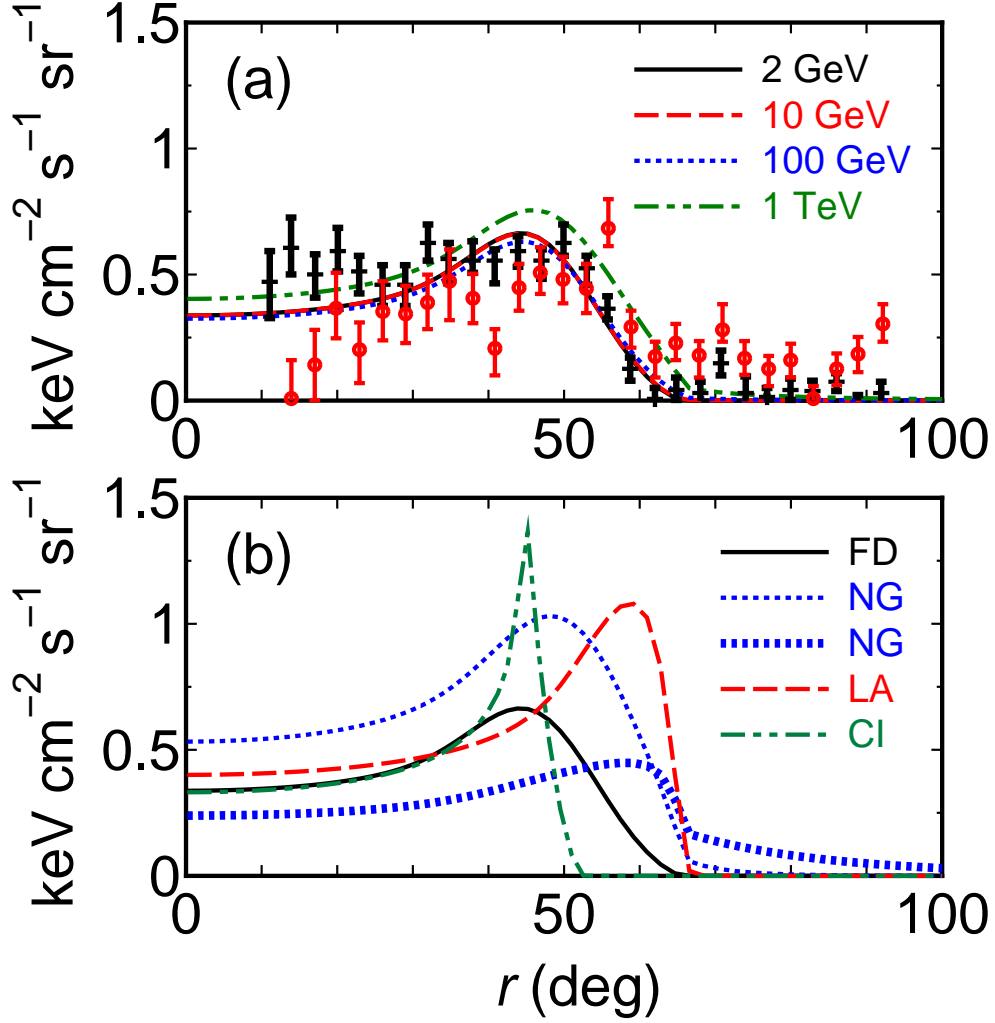


Fig. 1.— (a) Profiles of gamma-ray surface brightness at 2 GeV (solid), 10 GeV (dotted), 100 GeV (dashed), and 1 TeV (two-dotted dashed) for Model FD. Crosses and circles are the observations for the southern bubble by Su et al. (2010) in the 1–5 GeV band (cross) and 5–20 GeV band (circle), respectively. (b) Profiles of gamma-ray surface brightness at 2 GeV for Model FD (solid), at 2 GeV for Model NG (thin dotted), at 1 TeV for Model NG (thick dotted), at 2 GeV for Model LA (dashed), and at 2 GeV for Model CI (two-dotted dashed). For comparison, the surface brightness is multiplied by 0.5 for Model NG (2 GeV) and Model LA.

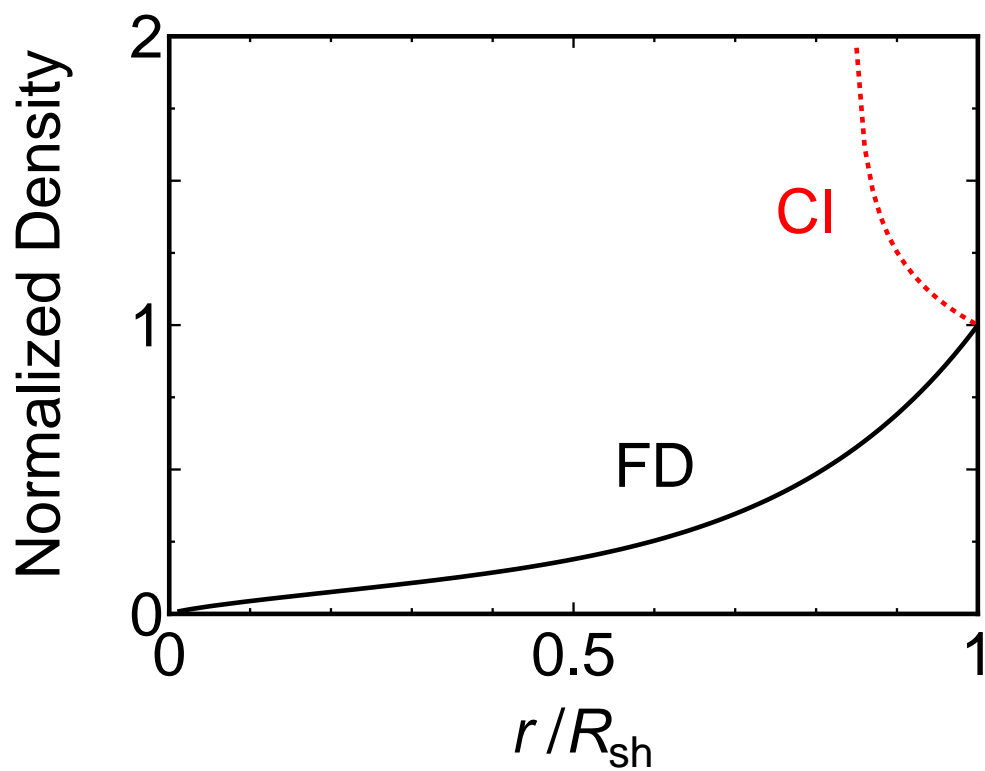


Fig. 2.— Gas density profiles within the bubble for Model FD (solid) and Model CI (dotted). The density is normalized by the value at $r = R_{\text{sh}}$.

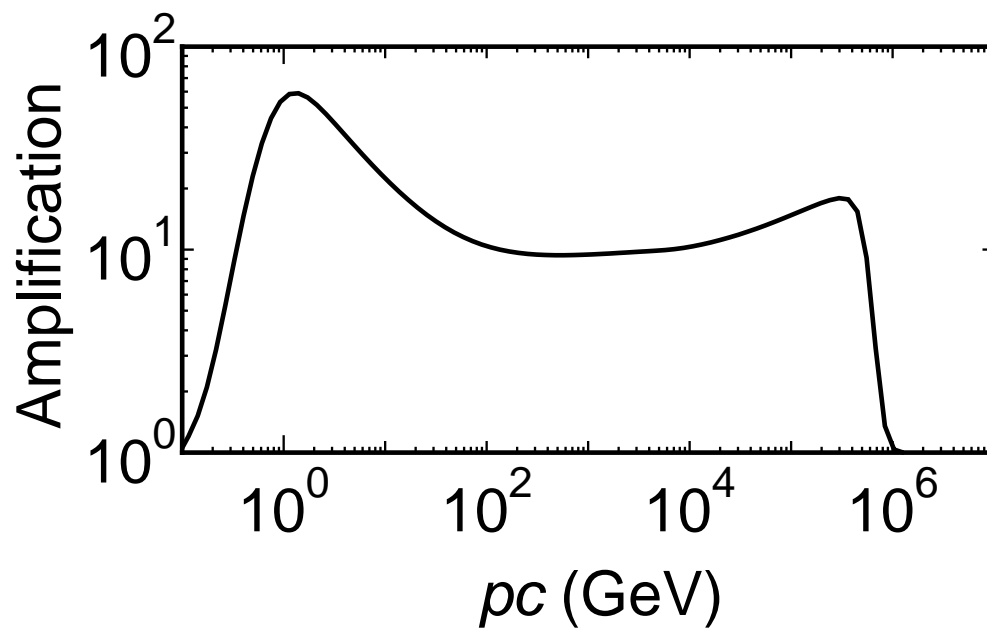


Fig. 3.— Amplification of magnetic fluctuations ψ/ψ_i at $r = R_{\text{sh},+}$ at $t = t_{\text{obs}}$ for Model FD.

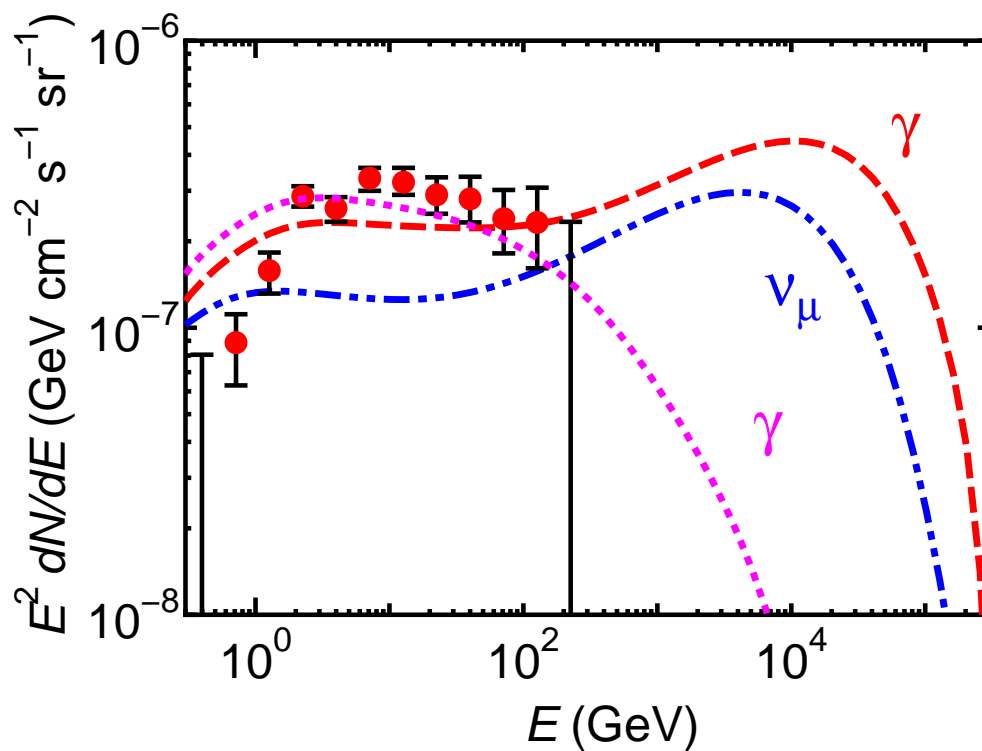


Fig. 4.— Gamma-ray (dashed) and neutrino ($\nu_\mu + \bar{\nu}_\mu$; two-dotted dashed) fluxes for Model FD. Dotted line is the gamma-ray spectrum when p_{\max} is small (see text). Filled circles are the observations (Su & Finkbeiner 2012).